

Optimizing NetGPT via Routing-Based Synergy and Reinforcement Learning

Yuxuan Chen, Rongpeng Li, Xianfu Chen, Celimuge Wu, Chenghui Peng, Zhifeng Zhao, and Honggang Zhang

Abstract—Large language model (LLM) agents at the network edge offer low-latency execution for routine queries. In contrast, complex requests often require the superior capability of cloud models, incurring higher latency and cost. To navigate this quality-cost trade-off under dynamic network conditions, we propose a cloud-edge synergy for NetGPT that integrates network-aware routing with on-edge self-improvement. Specifically, our framework routes structured tool-calling requests to cloud or edge agents via a novel scoring policy. We prove that, under mild regularity assumptions, the optimal routing rule admits a unique fallback threshold with monotone dependence on bandwidth and round-trip time (RTT). Concurrently, based on the dataset collected from requests routed to the cloud and corresponding responses, we instantiate a schema-preserving reinforcement learning (RL) to improve the capability of the edge agent. We analyze a supervised finetuning (SFT)-anchored composite objective that combines a reverse-KL trust-region step with a forward-KL realignment toward the SFT prior, explaining stability and constraining policy drift. Both the network-aware routing policy and the edge agent are updated coherently. Experiments across controlled network states and pricing schedules demonstrate smooth quality-cost frontiers, consistent gains of dynamic fallback thresholds over fixed policies, and sustained reductions in offloading while maintaining task success and schema-correct outputs.

Index Terms—Cloud-edge collaboration, large language models, tool-calling, task offloading, adaptive routing.

I. INTRODUCTION

The heterogeneous deployment of Large Language Models (LLMs) across the network is forming a NetGPT [1]. In this architecture, lightweight LLMs at the edge offer low latency but may struggle with complex queries, while more powerful and general-purpose cloud models lead to significant inference inefficiency and economic expenditure. The integration of external tools introduces even greater time-sensitivity [2] than vanilla LLM interactions [3]. Consequently, there is a compelling need for a cloud-edge synergy for NetGPT. Such a collaboration promises low-latency interactions at the edge with on-demand access to the high-quality reasoning of the cloud [4], [5].

Y. Chen and R. Li are with Zhejiang University, Hangzhou 310027, China, (email: {cxy00, lirongpeng}@zju.edu.cn).

X. Chen is with the Shenzhen CyberRay Network Technology Co., Ltd, China (e-mail: xianfu.chen@ieee.org).

C. Wu is with The University of Electro-Communications, Japan (e-mail: celimuge@uec.ac.jp).

C. Peng is with Huawei Technologies Co., Ltd., Shanghai 210026, China (email: pengchenghui@huawei.com).

Z. Zhao is with Zhejiang Lab, Hangzhou 310012, China as well as Zhejiang University, Hangzhou 310027, China (email: zhaozf@zhejianglab.org).

H. Zhang is with Macau University of Science and Technology, Macau 999078, China (email: hgzheng@must.edu.mo).

While devising a simple binary routing scheme (i.e., edge or cloud) sounds straightforward, an effective cloud-edge synergy is far more complicated. We face three key challenges. First, routing decisions are inherently state-dependent: the incremental quality from escalating a *hard* query to a stronger cloud model must be weighed against *network conditions* and *inference latency* [6]. Second, preference data collected from interacting with the cloud LLM can naturally be used to supervise the edge LLM [7] for capability improvement. Therefore, the developed routing policy should have the capability of automatically adapting to dynamic network conditions and concept drift [8]. Third, LLM agents must adhere to the tool-calling format (JSON) [9]. However, continuous improvement risks eroding schema adherence [10].

Existing paradigms cannot simultaneously solve these challenges. For example, cost-aware cascades [11]–[13] and preference-trained routers [14], [15] reduce average cost by sending *easy* queries to smaller models and escalating *hard* ones, but they typically operate as front-door or stage-wise mechanisms that are agnostic to link dynamics and seldom support continuous online improvement under schema constraints. Representation-learning routers further move beyond shallow classifiers: contrastive designs such as RouterDC [16] learn query-conditioned embeddings to score per-model utility, while graph-based approaches like GraphRouter [17] cast selection as inductive edge prediction on query-task-model heterogeneous graphs, improving generalization to unseen models and tasks, yet still treat latency and schema validity as exogenous variables. Distributed or multi-agent variants [18] emphasize ensemble specialization and coordination yet still decouple decisions from explicit network signals or rely on fixed acceptance rules. On the other hand, reinforcement learning (RL)-based online alignment pipelines — such as online direct preference optimization (DPO) [19] and iterative RL with human feedback (RLHF) workflows [20] — demonstrate how to continually refresh reward models and policies from streaming feedback under stability anchors, but they are typically designed for monolithic LLMs rather than tool-calling cloud-edge agents. Consequently, there still exists a methodological gap in optimizing NetGPT.

We address this gap by proposing a cloud-edge LLM pipeline that unifies tool-calling, network-aware routing, and online adaptation. Concretely, we use a unified router score trained from preference and quality signals. The score is produced by a lightweight reward model (RM) and is periodically refreshed using cached data from interactions with the cloud. Based on this score, a state-dependent fallback threshold is derived from network states like measured round-trip time

TABLE I: THE SUMMARY OF DIFFERENCES WITH RELATED LITERATURE.

References	Multi-stage	Tool Schema-aware	Pref. Quality	Network Aware	Online improv.	Brief description
[14]–[17]	○	○	●	○	○	Single-shot, front-door routing: a preference-trained scorer picks the model before generation.
[11], [12], [21]	●	○	●	○	○	Multi-stage cascade: apply a fixed quality threshold after each LLM to early-exit or escalate.
[22]	○	○	●	○	●	Contextual-bandit router: adapts model selection online under cost/quality uncertainty; agnostic to link dynamics and schema.
[13]	●	○	●	○	●	No explicit router: each LLM decides to forward/reject; trained for system utility.
[18]	○	●	●	○	○	Multi-agent routing with schema-aware coordination across specialized agents.
This work	●	●	●	●	●	Cloud-edge, tool-schema-aware multi-stage routing with state-dependent fallback thresholds enabling online adaptation.

Notation: ○ indicates not included; ● indicates fully included.

(RTT) and bandwidth. Simultaneously, the edge LLM policy is also updated via RL [23] with a cross-entropy supervised finetuning (SFT) anchor that preserves schema-correct tool-calling while ensuring stable updates. Furthermore, we analyze the theoretical simplicities and empirical advantages of the proposed pipeline. While highlighting the key differences with existing works in Table I, the main contributions of this paper are summarized as follows.

- We cast cloud-edge routing as a unified score-threshold policy whose acceptance boundary is an explicit function of measured network RTT and bandwidth. Under mild regularity assumptions on the confidence score, we theoretically prove that the optimal offloading rule admits a unique state-dependent fallback threshold and can be characterized by a first-order balance between the cloud’s marginal quality gain and its marginal cost. This yields monotone comparative statics to derive a network-aware fallback threshold.
- We unify tool-schema adherence with continual improvement by (i) using cached queries as on-policy supervision to refresh a lightweight RM, and (ii) optimizing the edge LLM policy via RL with an SFT anchor to maintain schema-correct tool-calling and stability during updates. By keeping routing decisions aligned with the evolving quality-latency-cost landscape, our design effectively tackles the underlying structural drift.
- We present an end-to-end evaluation under controlled network and pricing regimes, showing that dynamic, network-aware fallback thresholds consistently dominate fixed policies on the quality-cost frontier. Meanwhile, SFT-anchored on-device RL contributes to preserving task success and schema-correct tool-calling, and periodic RM refresh keeps the router calibrated and improves routing accuracy.

The remainder of the paper has been organized as follows. Section II reviews the background and related work. Section III describes the system model and formulates the optimization

problem. Section IV introduces the proposed dynamic fallback threshold mechanism and online self-improvement framework from both operational and theoretical perspectives. Section V presents the experimental results. Section VI concludes the paper.

Beforehand, major notations used throughout the paper are summarized in Table II.

II. RELATED WORK

A. LLM Routing and Selective Inference

Model selection across heterogeneous LLMs has rapidly evolved from early cost-aware cascades and difficulty-aware routers to theoretically grounded and benchmarked systems. Prototype cascades (e.g., [11]) reduce cost by answering *easy* queries with cheaper models and escalating *hard* cases to stronger models, showing sizable cost-quality gains but relying on offline heuristics and static thresholds. [15] formalizes two-model routing via a learned difficulty predictor that trades quality for cost and reports up to 40% fewer calls to the large model with negligible quality loss. On the supervised front, [14] trains a Bradley-Terry-Luce-style router on preference pairs mined from multi-model comparisons and evaluates routing under a cost/willingness-to-pay knob, and [24] standardizes multi-LLM routing evaluation and highlights the centrality of calibrated quality estimates.

Representation-learning routers broaden beyond shallow classifiers: [16] uses dual-contrastive training to predict per-model utility. [17] casts selection as inductive edge prediction on a query-model-task heterogeneous graph to improve generalization to unseen models and tasks. Concurrently, cascading receives theoretical treatment: [25] presents a unified analysis proving optimal strategies for both routing and cascades and introduces cascade routing, which outperforms either paradigm given accurate quality (and cost) estimators. Empirically oriented works refine the design space—e.g., [26] explores MIX-based cascades for reasoning workloads, [27] proposes dual-mode routing that blends pre-generation and cascade policies,

TABLE II: Notations used in the paper.

Notation	Description
x_i	Task/request index i
$H_{i,k}$	Context of task i at step k (history, tool outputs, etc.)
$u_{i,k}, u_{i,k}^*$	Structured actions produced respectively by the edge LLM and the cloud model (tool, args, thought)
g_ψ	Reward model (router score model) with parameters ψ
$s_{i,k}$	Router/reward-model score at (i, k)
$\tau(\cdot)$	Network-aware fallback threshold (runtime: $\tau(\hat{S}_{i,k})$)
$d_{i,k} \in \{E, C\}$	Routing decision at (i, k) : edge accept (E) or cloud offload (C)
$S_{i,k}, \hat{S}_{i,k}$	Latent network state at step k and its one-step-ahead estimate used in $\tau(\hat{S}_{i,k})$
$\text{RTT}_{i,k}$	Baseline round-trip path latency (propagation/queuing; size-independent) at step k
$\text{BW}_{i,k}$	Effective bandwidth at step k (determines transmission time T_{tx})
$\varepsilon_{i,k}, \Sigma$	Gaussian jitter and its scale in the Gauss–Markov model for time-varying network state
L_E, L_C	Latency of a local step (edge) and a cloud-offloaded step (uplink-compute-downlink)
$L_{i,k}, L(x_i)$	Realized latency at (i, k) ; end-to-end latency of task i
$N_{i,k}$	Token usage of the cloud model at (i, k)
$C_{i,k}, C(x_i)$	Step cost and total task cost (latency penalty + cloud cost)
$Q_{i,k}, Q(x_i)$	Step quality in $[0, 1]$ and average task quality
$J(x)$	Utility measuring the quality-cost trade-off
λ	Trade-off coefficient on cost
π_θ	Edge LLM policy with parameters θ
π_{SFT}	Supervised reference policy used for SFT anchoring
$r_{i,k}$	Learning reward for online updates at (i, k)
$\kappa(S)$	Network scaling of cloud cost under state S in comparative statics ($\Delta C_S = \kappa(S) \Delta C$)
$\rho(s)$	Local benefit–cost ratio at score s
$f(s)$	Density of the confidence score s
C_{tok}	Unit price per cloud token used in the monetary-cost term
$\alpha_{\text{RTT}}, \beta_{\text{BW}}, \gamma_{\text{hist}}$	Coefficients in the linear dynamic fallback threshold (RTT/BW/history sensitivities)
$f_\omega(\cdot), \omega$	Lightweight neural router (PolicyNet) and its parameters
γ	Discount factor in the on-device RL objective
$\rho_{i,k}$	PPO importance ratio
$A_{i,k}$	Advantage estimate used in PPO
ϵ	PPO clipping range in the surrogate objective
β_{KL}	Reverse-KL penalty coefficient in PPO
η	Forward-KL anchor (SFT realignment) weight
π_t	Current policy at iteration t in the two-stage update
$T_{i,k}$	Cached tuple $(x_i, H_{i,k}, u_{i,k}, u_{i,k}^*, s_{i,k})$
$\mathcal{B}_{\text{RM}}, \mathcal{B}_{\text{RL}}$	Caches storing on-policy samples for RM and PPO updates

and [28] augments routing with adaptive additional computation for small models to yield test-time optimal compute. Bandit and non-parametric perspectives further question router complexity: [22] frames selection as a contextual bandit to adapt to cost/quality uncertainty, while [29] shows strong performance of kNN-based routing versus learned routers on standardized benchmarks, underscoring the role of locality in embedding space. [18] extends routing to multi-agent settings by jointly choosing collaboration modes, allocating roles, and routing queries across heterogeneous LLMs, but still abstracts away time-varying network effects and offers limited online

adaptation under bandit feedback—constraints that reduce suitability for cloud-edge deployments.

Despite progress, several structural limitations persist for our cloud-edge setting. First, network unawareness is pervasive: most studies treat *cost* as API price or FLOPs and either ignore latency/bandwidth or treat them as constants; even works that model cost explicitly rarely integrate time-varying link measurements into the decision boundary, and recent surveys acknowledge that many routers ignore latency in practice [21]. Second, online self-improvement is rarely a primary design goal: routers are commonly trained offline with full supervision (quality labels for all models) and lack the capability of online adaptation. Third, schema-constrained tool-calling—now standard in agentic pipelines—poses a stability constraint largely absent from routing benchmarks. Motivated by these gaps, we propose a network-aware, schema-preserving routing pipeline with continual improvement. It uses a unified score to govern edge acceptance and offload, adapts fallback thresholds explicitly to measured RTT and bandwidth, and reuses cached escalated queries to refresh the router’s reward model and the edge LLM policy.

B. Online Learning and Adaptive Optimization in Networked Agents

In the LLM era, online alignment seeks to improve models during deployment under bandit feedback, distribution shift, and tight latency, rather than relying solely on offline preference corpora. [30] further formalizes online preference optimization with equivalences to Nash mirror descent and demonstrates how to update policies from streaming preferences with Kullback–Leibler (KL) control. To curb catastrophic forgetting in continual DPO, [19] introduces an online DPO method with a fast-slow memory that decouples rapid adaptation from a stable anchor to preserve earlier competencies. Beyond pure DPO, self-play and self-rewarding methods close the loop by generating rewards on the fly. [31] demonstrates that LLM-as-a-Judge can bootstrap iterative DPO and jointly improve both the model and its internal judge. To mitigate judge drift, [32] adds consistency regularization across iterations, improving reward reliability in self-rewarding pipelines. A game-theoretic perspective is provided by [33], which frames alignment as a constant-sum game and proves convergence of iterative self-play preference optimization updates.

Several works study robustness and grouping in continual alignment. [34] seeks worst-group improvements to avoid regressing minority preferences when updating online. On the RL side, [35] presents a group-relative PPO variant that removes the critic and estimates baselines from group scores, offering a lighter-weight alternative for iterative preference-driven improvement in reasoning-heavy tasks. From a systematic perspective, [20] describes online iterative RLHF workflows that construct proxy preference models, generate on-policy data, and repeat align-evaluate-deploy cycles, reporting consistent gains over offline pipelines. A complementary theoretical analysis is provided by [36], which generalizes online RLHF to preference oracles beyond Bradley–Terry assumptions and develops sample-efficient procedures for querying and updating on the fly.

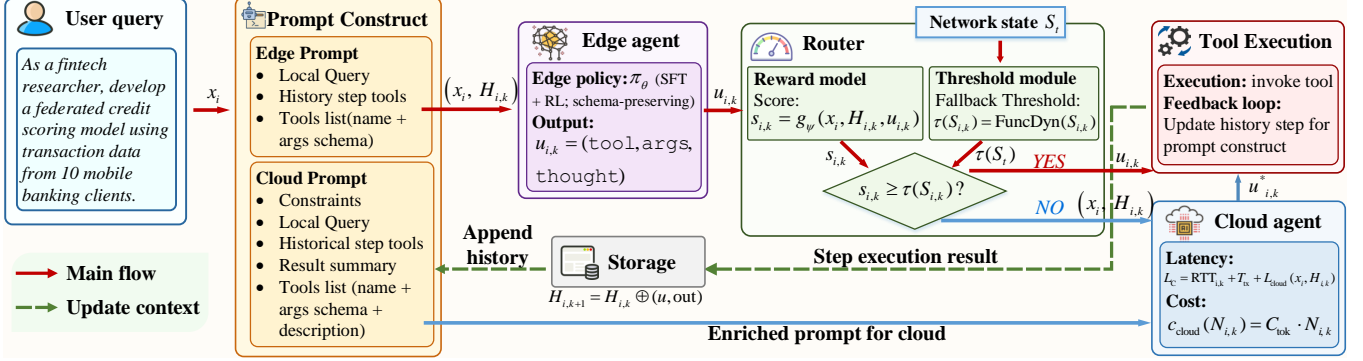


Fig. 2: Online-stage of the proposed pipeline.

B. Problem Formulation

For each task x_i , the task-level quality and cost are defined by aggregating per-step quantities separately:

$$Q(x_i) = \frac{1}{K_i} \sum_{k=1}^{K_i} Q_{i,k}, \quad C(x_i) = \sum_{k=1}^{K_i} C_{i,k}. \quad (10)$$

We then define a utility function that balances these two metrics:

$$J(x_i) = Q(x_i) - \lambda C(x_i), \quad \lambda > 0. \quad (11)$$

The trade-off coefficient λ controls the tolerance for latency and cost under given quality priorities.

The overall optimization objective is to maximize the expected utility across all tasks by jointly learning the network-aware fallback threshold function $\tau(\cdot)$ and the edge LLM policy parameters θ :

$$\max_{\tau(\cdot), \theta} \mathbb{E}_{x \sim \mathcal{D}}[J(x)] = \max_{\tau(\cdot), \theta} \mathbb{E}[Q(x) - \lambda C(x)]. \quad (12)$$

Here, $x \sim \mathcal{D}$ denotes sampling a task from the deployment-time workload distribution; $\tau(\cdot)$ governs routing under the observed network state S ; and θ parameterizes the on-device policy that generates structured tool calls.

The key difficulty to solve (12) lies in coupling short-term network adaptation with long-term model improvement. Existing formulations typically isolate routing from model adaptation [14], [16], and often assume fixed or exogenous communication costs or static model behavior [11], [15]. Nevertheless, decoupling of network-aware fallback thresholds and underlying model improvement could significantly compromise the efficiency. Instead, the fallback threshold $\tau(\cdot)$ should react to instantaneous variations of the network state S while the edge LLM π_θ and RM g_ψ continuously improve according to observed data during online inference. These two processes operate on different time scales but jointly determine the system's stability and efficiency.

IV. METHOD

To maximize the expected utility J , we combine dynamic fallback threshold adaptation with schema-preserving RL, both guided by a unified router score. The former responds rapidly to changing network states, while the latter gradually improves

the edge LLM's competence under data drift without compromising tool-schema correctness.

A. Dynamic Fallback Thresholds

To characterize the routing behavior under varying network states, we first analyze the threshold-based decision rule and its optimality conditions. Without loss of generality, for each request with confidence score s , we assume that the edge execution yields quality Q_E and cost C_E , while the cloud execution yields Q_C and C_C . We define the marginal cloud-edge differences:

$$\Delta Q(s) \triangleq \mathbb{E}[Q_C - Q_E | s], \quad \Delta C(s) \triangleq \mathbb{E}[C_C - C_E | s]. \quad (13)$$

Intuitively, $\Delta Q(s)$ is the expected quality gain (if any) from escalating a score- s request to the cloud rather than accepting the edge inference, while $\Delta C(s)$ is the induced extra cost (e.g., latency, transmission, cloud inference). Let $f(s)$ be the density of the confidence score s , and we make the following assumption.

Assumption 1 (Regularity of the score). *The confidence score s admits an absolutely continuous distribution with density f that is strictly positive on the relevant support.*

Assumption 1 only requires conditional continuity with respect to the score, but does not specify any particular parametric model for (Q_E, Q_C, C_E, C_C) . Therefore, it can be easily met.

We now express the sensitivities of $(Q(\tau), C(\tau))$ with respect to the fallback threshold τ .

Lemma 1 (Frontier sensitivities). *Under Assumption 1,*

$$\frac{dQ}{d\tau}(\tau) = f(\tau) \Delta Q(\tau), \quad \frac{dC}{d\tau}(\tau) = f(\tau) \Delta C(\tau). \quad (14)$$

Proof. By the definition of the score-threshold policy,

$$Q(\tau) = \int_{\tau}^{\infty} \mathbb{E}[Q_E | s] f(s) ds + \int_{-\infty}^{\tau} \mathbb{E}[Q_C | s] f(s) ds. \quad (15)$$

Applying Leibniz's rule and continuity yields

$$\begin{aligned}\frac{dQ}{d\tau}(\tau) &= -\mathbb{E}[Q_E \mid s = \tau]f(\tau) + \mathbb{E}[Q_C \mid s = \tau]f(\tau) \\ &= f(\tau)\Delta Q(\tau).\end{aligned}\quad (16)$$

The identity for $dC/d\tau$ is analogous. \blacksquare

A direct corollary of Lemma 1 is the *frontier slope identity*:

$$\frac{dQ}{dC}(\tau) = \frac{\Delta Q(\tau)}{\Delta C(\tau)} = \rho(\tau), \quad (17)$$

i.e., the slope of the achievable (Q, C) frontier at fallback threshold τ equals the local benefit–cost ratio of requests with score $s = \tau$.

Assumption 2 (Informativeness of the score). *The cloud-edge marginal cost differential $\Delta C(s)$ is strictly positive on its support; $\Delta Q(\cdot)$ and $\Delta C(\cdot)$ are continuous with the ratio $\rho(s) \triangleq \Delta Q(s)/\Delta C(s)$ strictly decreasing in s .*

Assumption 2 is natural: as the confidence score increases, the cloud's incremental benefit relative to the edge diminishes faster than its incremental cost, making a single switch optimal.

We next solve the scalar optimization $\max_{\tau} J(\tau)$ and show the uniqueness of the optimal fallback threshold τ^* .

Theorem 1 (Unique optimal fallback threshold (first-order balance)). *Under Assumption 1 and Assumption 2, the score-threshold policy is optimal among all measurable policies that depend only on the score, and the maximizer τ^* of $J(\tau)$ is unique. It is characterized by the first-order balance*

$$\Delta Q(\tau^*) = \lambda \Delta C(\tau^*), \quad \text{sign}(J'(\tau)) = \text{sign}(\rho(\tau) - \lambda). \quad (18)$$

Proof. By Lemma 1,

$$\begin{aligned}J'(\tau) &= \frac{dQ}{d\tau}(\tau) - \lambda \frac{dC}{d\tau}(\tau) \\ &= f(\tau)(\Delta Q(\tau) - \lambda \Delta C(\tau)) \\ &= f(\tau)\Delta C(\tau)(\rho(\tau) - \lambda).\end{aligned}\quad (19)$$

Assumption 1 and Assumption 2 ensure $f(\tau) > 0$ and $\Delta C(\tau) > 0$, respectively. Hence, the sign of $J'(\tau)$ is the sign of $\rho(\tau) - \lambda$. Because $\rho(\cdot)$ is strictly decreasing and continuous, there exists a unique τ^* satisfying $\rho(\tau^*) = \lambda$; at that point $J'(\tau^*) = 0$, and strict monotonicity of ρ implies J' changes sign, yielding a unique maximizer τ^* . Optimality of the fallback threshold structure among score-based policies follows from the single-crossing of $\rho(\cdot)$. Finally, by Lemma 1, the frontier slope at τ equals $dQ/dC = \rho(\tau)$, so it equals λ at τ^* . \blacksquare

Remark 1. *Under the mild regularity conditions of Theorem 1, the Pareto frontier traced by $\tau \mapsto (Q(\tau), C(\tau))$ is strictly monotone and differentiable. Meanwhile, the optimal routing policy possesses three interpretable properties: (i) the optimal measurable score-based policy is threshold-shaped; (ii) the fallback threshold τ^* is unique and satisfies a first-order balance between the marginal expected quality gain and the*

marginal offload cost; and (iii) at the unique maximizer τ^ , its tangent slope equals λ .*

This result provides a principled basis for incorporating network state S (e.g., bandwidth, RTT) into the fallback threshold τ , which we extend to the state-aware case below. Our goal is to characterize how the optimizer $\tau^*(S)$ of $J(\tau; S) = Q(\tau; S) - \lambda C(\tau; S)$ shifts with S .

Assumption 3 (Separable network impact). *There exists a strictly positive, continuous scaling $\kappa(S)$ such that $\Delta C_S(s) = \kappa(S) \Delta C(s)$ for all s ; moreover, the marginal quality gain is governed by task difficulty captured by the score and is not distorted by the link, i.e., $\Delta Q_S(s) = \Delta Q(s)$.*

By Assumption 3 and Theorem 1, the optimal fallback threshold $\tau^*(S)$ is characterized by

$$\Delta Q(\tau^*(S)) = \lambda \Delta C_S(\tau^*(S)) = \lambda \kappa(S) \Delta C(\tau^*(S)), \quad (20)$$

or equivalently $\rho(\tau^*(S)) = \lambda \kappa(S)$.

Theorem 2 (Network influence on τ^*). *Under Assumption 2 and Assumption 3, if $\kappa(S_1) > \kappa(S_2)$ then $\tau^*(S_1) < \tau^*(S_2)$.*

Proof. Start from the first-order condition at state S :

$$\rho(\tau^*(S)) = \lambda \kappa(S). \quad (21)$$

Pick S_1, S_2 with $\kappa(S_1) > \kappa(S_2)$. Then

$$\lambda \kappa(S_1) > \lambda \kappa(S_2). \quad (22)$$

By strict monotonic decrease of $\rho(\cdot)$ (Assumption 2), the equation $\rho(\tau) = \lambda \kappa(S)$ has a unique solution and the solution moves in the *opposite* direction of the right-hand side. Hence

$$\rho(\tau^*(S_1)) > \rho(\tau^*(S_2)) \implies \tau^*(S_1) < \tau^*(S_2), \quad (23)$$

which proves the theorem. \blacksquare

Remark 2. *Theorem 2 implies that if κ is strictly decreasing in available bandwidth BW and strictly increasing in RTT or cloud-unit price C_{tok} , then τ^* is strictly increasing in BW and strictly decreasing in RTT and C_{tok} .*

Corollary 1 (Local sensitivity of $\tau^*(S)$). *Suppose ρ is continuously differentiable and $\rho'(\tau) \triangleq \frac{d\rho}{d\tau} < 0$. Then τ^* is continuously differentiable in κ , and*

$$\frac{d\tau^*}{d\kappa}(S) = \frac{\lambda}{\rho'(\tau^*(S))} < 0. \quad (24)$$

Proof. Define the residual:

$$F(\tau, \kappa) \triangleq \rho(\tau) - \lambda \kappa. \quad (25)$$

At $(\tau^*(S), \kappa(S))$, the optimality condition gives $F(\tau^*(S), \kappa(S)) = F_\tau(\tau^*, \kappa) d\tau^* + F_\kappa(\tau^*, \kappa) d\kappa = 0$, which implies:

$$\frac{d\tau^*}{d\kappa} = -\frac{F_\kappa}{F_\tau} = -\frac{-\lambda}{\rho'(\tau^*)} = \frac{\lambda}{\rho'(\tau^*)}. \quad (26)$$

This establishes the corollary. \blacksquare

Finally, the frontier's local geometry inherits the same

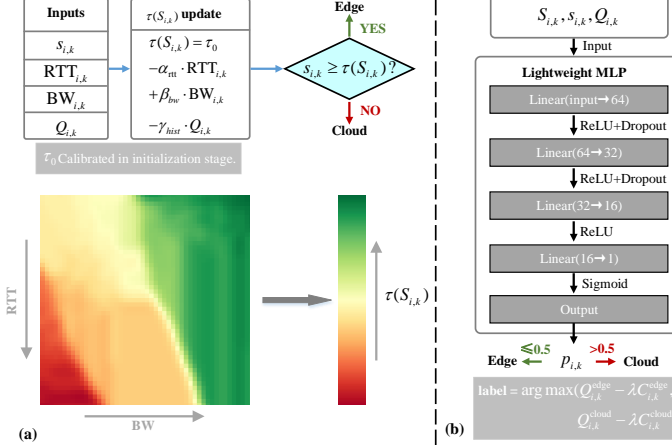


Fig. 3: Runtime routing modules and adaptive fallback thresholding. (a) Dynamic fallback threshold controller $\tau_{i,k} = f_\phi(S_{i,k}, \hat{Q}_{i,k})$, initialized from the offline-calibrated τ_0 and adjusted by the current network state ($RTT_{i,k}, BW_{i,k}$) and recent quality $\hat{Q}_{i,k}$. The heatmap shows how network state variables shape $\tau_{i,k}$, with $\hat{Q}_{i,k}$ fixed at its validation mean. (b) Lightweight router f_ω (PolicyNet) takes $[S_{i,k}, s_{i,k}, \hat{Q}_{i,k}]$ and outputs routing probability $p_{i,k}$; decisions follow $p_{i,k} \leq 0.5 \Rightarrow$ Edge, $p_{i,k} > 0.5 \Rightarrow$ Cloud.

parameterization: for each fixed S and fallback threshold τ ,

$$\frac{dQ}{dC}(\tau; S) = \frac{\Delta Q(\tau)}{\Delta C_S(\tau)} = \frac{\rho(\tau)}{\kappa(S)}. \quad (27)$$

Therefore, improving network states (smaller $\kappa(S)$) steepens the attainable quality-cost slope at the same fallback threshold. Together with the first-order balance $\rho(\tau^*(S)) = \lambda \kappa(S)$, this shows that the network state shifts the optimal fallback threshold monotonically. In practice, this motivates either a linearized functional mapping (FuncDyn) or a lightweight one-hidden-layer router (PolicyNet).

- *FuncDyn*: It computes the fallback threshold $\tau_{i,k}$ as a smooth function of the observed link condition and recent execution history:

$$\tau_{i,k} = \tau_0 - \alpha_{RTT}RTT_{i,k} + \beta_{BW}BW_{i,k} - \gamma_{hist}\hat{Q}_{i,k}, \quad (28)$$

Here τ_0 denotes the base fallback threshold level obtained from the initialization procedure described in Appendix A, and serves as the reference point adjusted by the observed network state. $\hat{Q}_{i,k}$ denotes a running estimate of $Q_{i,k}$.

As shown in Fig. 3(a), $\tau_{i,k}$ increases with bandwidth and decreases with RTT, consistent with the comparative statics established in Theorem 2.

- *PolicyNet*: It eliminates the explicit fallback threshold and learns a small neural policy that directly outputs the routing decision. Given the feature tuple $(S_{i,k}, s_{i,k}, \hat{Q}_{i,k})$, the PolicyNet predicts the probability of routing to the cloud:

$$p_{i,k} = \sigma(f_\omega(S_{i,k}, s_{i,k}, \hat{Q}_{i,k})) \geq 0.5, \quad (29)$$

where the neural network $f_\omega(\cdot)$ is a compact MLP (4 layers, $\approx 2,900$ parameters), ensuring it can be deployed efficiently on the edge device. The neural network $f_\omega(\cdot)$ can be trained following a standard logistic objective,

$$\mathcal{L}_{\text{policy}}(\omega) = \mathbb{E}[-y_{i,k} \log p_{i,k} - (1 - y_{i,k}) \log(1 - p_{i,k})], \quad (30)$$

where the training label $y_{i,k} = \arg \max (Q_{i,k}^{\text{edge}} - \lambda C_{i,k}^{\text{edge}}, Q_{i,k}^{\text{cloud}} - \lambda C_{i,k}^{\text{cloud}})$.

B. Online Self-Improvement

After initialization, the edge agent continues to refine itself (i.e., π_θ), contingent on the unified score signal $s_{i,k}$ and shared cached edge–cloud pairs collected during deployment¹. At step (i, k) , the router score acts as the immediate reward by

$$r_{i,k} = s_{i,k} = g_\psi(x_i, H_{i,k}, u_{i,k}). \quad (31)$$

The goal is to maximize the expected discounted return in

$$\max_{\theta} \mathbb{E}_{\pi_\theta} \left[\sum_k \gamma^k r_{i,k} \right], \quad 0 < \gamma \leq 1. \quad (32)$$

The discount factor γ controls how strongly future rewards affect current updates.

Commonly, we follow

$$\begin{aligned} \text{(RL-KL)} \quad \tilde{\pi}_{t+1} &= \arg \max_{\pi} \underbrace{\mathbb{E}_{(s,a) \sim d_{\pi_t}} [A_{\pi_t}(s, a) \log \pi(a|s)]}_{\text{policy improvement}} \\ &\quad - \eta_t \text{KL}(\pi \parallel \pi_t). \end{aligned} \quad (33)$$

and apply a clipped PPO update [23] by optimizing:

$$\begin{aligned} \mathcal{L}_{\text{RL}}(\theta) &= \mathbb{E} \left[\min(\rho_{i,k} A_{i,k}, \text{clip}(\rho_{i,k}, 1 - \epsilon, 1 + \epsilon) A_{i,k}) \right] \\ &\quad - \beta_{\text{KL}} \text{KL}(\pi_\theta \parallel \pi_{\text{old}}), \end{aligned} \quad (34)$$

where

$$\rho_{i,k} = \frac{\pi_\theta(u_{i,k} \mid x_i, H_{i,k})}{\pi_{\text{old}}(u_{i,k} \mid x_i, H_{i,k})},$$

$A_{i,k}$ is the advantage estimate from rewards, ϵ indicates the clipping range, and β_{KL} is the KL penalty coefficient controlling the update size.

On the other hand, to maintain structured outputs, every M PPO updates are followed by a short SFT anchoring step:

$$\begin{aligned} \text{(SFT-CE)} \quad \pi_{t+1} &= \arg \min_{\pi} \mathbb{E}_{s \sim \mathcal{D}_{\text{SFT}}} \left[\underbrace{H(\pi_{\text{SFT}}(\cdot|s), \pi(\cdot|s))}_{\text{KL}(\pi_{\text{SFT}} \parallel \pi) + \text{const}} \right]. \end{aligned} \quad (35)$$

where π_{SFT} is the frozen supervised model. This projection keeps the tool schema correct while allowing the edge LLM policy to improve. Over time, π_θ learns to approach the cloud’s performance with reduced cost.

The first stage (RL-KL) performs a KL-regularized trust-region update that delivers stable policy improvement for a regularized MDP [39]. Meanwhile, the second stage (SFT-CE) applies an SFT-anchored cross-entropy projection that

¹We leave the details of caching setup in Appendix B.

pulls the policy back toward the SFT manifold to preserve formatting/tool-calling habits [40]. Jointly, the alternation can be viewed as block-coordinate ascent on a composite regularized objective:

$$\begin{aligned} J_{\eta, \mu}(\pi; \pi_t, \pi_{\text{SFT}}) &= \mathbb{E}_{s \sim d_{\pi_t}, a \sim \pi(\cdot|s)} [A(s, a)] \\ &\quad - \eta \mathbb{E}_{s \sim d_{\pi_t}} [\text{KL}(\pi(\cdot|s) \parallel \pi_t(\cdot|s))] \\ &\quad - \mu \mathbb{E}_{s \sim d_{\pi_t}} [\text{KL}(\pi_{\text{SFT}}(\cdot|s) \parallel \pi(\cdot|s))]. \end{aligned} \quad (36)$$

Here $A(s, a)$ is the same advantage estimator as defined in Eq. (34), and d_{π_t} denotes the discounted state distribution under the current policy.

Similar to the initialization method in Appendix A, the reward model is incrementally updated using the same pairwise ranking loss with schema penalty as Eq. (38). Fine-tuning is performed in small batches with early stopping to prevent reward drift. This incremental refresh keeps g_ψ aligned with the evolving edge LLM policy π_θ and the time-varying network state S , ensuring that the router signal $s_{i,k}$ remains consistent and informative.

Finally, we summarize the whole procedure for the cloud-edge synergy in Algorithm 1.

V. PERFORMANCE EVALUATION

A. Experimental Setup

We consider a NetGPT scenario with a heterogeneous tool-calling stack where the edge runs DeepSeek-R1-Distill-Qwen-7B (FP32, non-quantized) and the cloud uses DeepSeek-V3.2-Exp. Both models are required to emit structured tool calls with a tool name, arguments, and a brief thought trace, but we use different prompting schemes at the edge and in the cloud. At the edge, we use a compact schema that includes the current query, tool names from previous steps, and the list of currently available tools with their argument slots. In the cloud, we use a ReAct-style prompt [3] with richer task instructions and full tool and argument descriptions to enforce the desired reasoning pattern and output format.

At the edge, we optimize the local LLM with PPO [23], using the unified router score as a scalar reward. The score $s_{i,k}$ is produced by a lightweight reward model g_ψ instantiated on *Qwen2.5-1.5B-Instruct*, fine-tuned on comparison judgments favor cloud-level tool-calling quality and to penalize schema or format violations. During deployment, g_ψ serves as the scoring module of the router, while the routing policy leverages $s_{i,k}$, the current network state $S_{i,k}$, and the running quality estimate $\hat{Q}_{i,k}$ to decide whether to continue execution on the edge or offload the next step to the cloud.

Workloads are drawn from a private corpus of tool-calling tasks that matches our target skill mix. From this corpus², we sample 8,000 examples for SFT-based initialization of the edge LLM for stabilizing schema-compliant tool-calling, 2,000 examples to train the reward model, and 8,000 tasks

²As described in Section IV and Appendix B, only cloud-offloaded steps are logged and reused.

Algorithm 1 Network-Aware Routing and Online Self-Improvement

Inputs: dataset \mathcal{D} , schema \mathcal{S} , trade-off λ , link logs, edge LLM policy π_{SFT} , reward model g_ψ , horizon M .

Outputs: updated π_θ , $\tau(\cdot)$ or f_ω , refreshed g_ψ .

Offline Initialization

- 1: Obtain π_{SFT} by Eq. (37)
- 2: Obtain g_ψ by Eq. (38)
- 3: Obtain τ_0 by Eq. (40)
- 4: Set $\pi_\theta \leftarrow \pi_{\text{SFT}}$

Online Routing and Self-Improvement

- 1: **for** each task i **do**
- 2: $k \leftarrow 1$, context $H_{i,1}$
- 3: **while** task i not finished **do**
- 4: $u_{i,k} \sim \pi_\theta(\cdot|x_i, H_{i,k})$
- 5: Obtain $s_{i,k} = g_\psi(x_i, H_{i,k}, u_{i,k})$ by Eq. (2)
- 6: Obtain $\tau_{i,k}$ by Eq. (28) or Obtain $p_{i,k}$ by Eq. (29)
- 7: **if** $s_{i,k} \geq \tau_{i,k}$ or $p_{i,k} \geq 0.5$ **then**
- 8: Execute $u_{i,k}$ locally
- 9: **else**
- 10: Query cloud $\Rightarrow u_{i,k}^*$
- 11: Obtain $C_{i,k}$ by Eq. (8)
- 12: Store $(x_i, H_{i,k}, u_{i,k}, u_{i,k}^*, s_{i,k}, S_{i,k})$ in \mathcal{B}_{RM}
- 13: **end if**
- 14: Compute $Q_{i,k}$ by Eq. (9)
- 15: Compute $L_{i,k}$ by Eq. (6)
- 16: Update history $\hat{Q}_{i,k} \leftarrow (1 - \beta)\hat{Q}_{i,k-1} + \beta Q_{i,k}$
- 17: Update $H_{i,k+1}$ by Eq. (42)
- 18: Add $(x_i, H_{i,k}, u_{i,k}, r_{i,k} = s_{i,k})$ to \mathcal{B}_{RL}
- 19: $k \leftarrow k + 1$
- 20: **end while**
- 21: **end for**
- 22: **for** each idle window **do**
- 23: Update π_θ by PPO using Eq. (34) on \mathcal{B}_{RL}
- 24: **if** every M steps **then**
- 25: Align π_θ to π_{SFT} by Eq. (35)
- 26: **end if**
- 27: Update g_ψ using incremental RM training (Eq. (2)) on \mathcal{B}_{RM}
- 28: Recalibrate $\tau_{i,k}$ or f_ω using latest $(S_{i,k}, \hat{Q}_{i,k})$
- 29: **end for**
- 30: **return** π_θ , $\tau(\cdot)$ or f_ω , g_ψ

for inference experiments and simulated continual improvement. Task difficulty scales with input length and tool-calling complexity: each instance exposes 10–20 candidate tools and includes between 0 and 8 previously executed steps. During evaluation, requests are processed step-wise and metrics are aggregated at the task level. To couple routing decisions with network conditions, each request samples a throughput BW (Mbps) and a round-trip time RTT (ms) from one of three regimes:

- GOOD: BW $\in [120, 200]$, RTT $\in [20, 40]$;

“As an edge-device engineer, implement federated learning across 50 IoT sensors collecting temperature and humidity data, using a lightweight CNN model with differential privacy guarantees..”

Prompt Construct

```
{
  "query": "As an edge-device engineer, implement...",
  "completed_steps": ["initialize_nodes"],
  "available_tools": [
    "initialize_nodes(node_count, model_class, dataset_name)",
    "Simulate_topology(node_count, Bandwidth_limits, latencies)",
    "...",
    "aggregate_global_model_secure_agg(local_models, ...)",
    "finish()"
  ]
}
```

LLM

```
{
  "name": "simulate_topology",
  "args": {
    "node_count": 51,
    "bandwidth_limits": {"value": 10, "count": 50},
    "latencies": {"value": 5, "count": 50}
  },
  "thought": "A star topology suits IoT sensors with one coordinating server. Set bandwidth to 10 Mbps and latency to 5 ms."
}
```

Tool execution

Fig. 4: Example of structured text flow across stages.

- MID: $BW \in [30, 80]$, $RTT \in [40, 80]$;
- BAD: $BW \in [5, 15]$, $RTT \in [80, 130]$.

This design aligns our three buckets with established QoS envelopes: according to the ITU-T Y.1541 [37] end-to-end objectives, 20 – 40 ms RTT reflects metro/near-region paths, while 40 – 80 ms RTT corresponds to typical regional paths, and 80 – 130 ms RTT indicates long-haul yet standards-consistent paths. For bandwidth, we sample a link rate in Mbps as a controlled variable but interpret its effect through the TCP bandwidth-delay-product (BDP) rationale (RFC 6349) [38], i.e., GOOD/MID/BAD correspond to low-/moderate-/high-BDP regimes that govern achievable throughput and window sizing. We model time-varying network state via a one-step Gauss-Markov update $S_{i,k} = S_{i,k-1} + \varepsilon_{i,k}$, where $\varepsilon_{i,k} \sim \mathcal{N}(0, \Sigma^2)$. For time-correlated links, such a method underpins widely used network/wireless mobility abstractions [41].

We study two policies: *FuncDyn* constructs a rule-based dynamic fallback threshold $\tau_{i,k}$ from the normalized round-trip time $RTT_{i,k}$, bandwidth $BW_{i,k}$, and a historical quality $\hat{Q}_{i,k}$, and offloads when $s_{i,k} > \tau(RTT_{i,k}, BW_{i,k}, \hat{Q}_{i,k})$. *PolicyNet* is a compact four-layer MLP that takes as input $x_{i,k} = (S_{i,k}, s_{i,k}, \hat{Q}_{i,k})$ and outputs a binary cloud-edge

routing decision. For comparison, we evaluate two routing baselines. *RouteLLM* [14] is a learned one-shot router that, given an input query, makes a single binary choice—answer on the edge or offload to a stronger model—and keeps this choice fixed throughout multi-step tool calling. *FrugalGPT* [11] implements a fixed fallback threshold cascade, where requests are passed from smaller to larger models according to a static acceptance rule. All training and batched inference run on 8× NVIDIA A800 (80 GB) GPUs.

Metrics include *utility* J , *composite quality* Q , *total cost* C , and *offload rate* (fraction of requests routed to the cloud). Unless otherwise stated, all metrics are reported as averages over the 8,000 evaluation tasks. We record latency components but report normalized costs so that Q and C remain commensurate under the chosen λ . In addition, for frontiers and sensitivity analyses, we sweep τ over a dense grid; for long traces, we interleave regimes to emulate time-varying links.

B. Adaptive Routing under Time-Varying Links

We compare our dynamic controllers (FuncDyn and PolicyNet) with RouteLLM, FrugalGPT, and two additional baselines (All Edge and All Cloud) across GOOD/MID/BAD regimes, and Fig. 5 presents the corresponding results. It shows FuncDyn yields the highest J while keeping the offload rate moderate, reflecting effective state-aware acceptance. PolicyNet attains the highest Q with higher offload and cost. In contrast, FrugalGPT ranks between the dynamic controllers and RouteLLM across regimes. Under regime switches, RouteLLM yields the lowest utility J , while our dynamic controllers remain top-performing. Together with the baselines All Edge and All Cloud, the comparison indicates that coupling the router with both execution agents yields a larger utility J across GOOD/MID/BAD.

We evaluate routing under interleaved network conditions by tracking the per-request utility ($J = Q - \lambda C$) over a long trace. Fig. 6 plots the step-level J together with its windowed mean for a dynamic, network-aware fallback threshold and for a fixed fallback threshold representative of a static acceptance policy. Across regime switches, the dynamic fallback threshold maintains a consistently higher average J : when the link deteriorates, the controller lowers the acceptance boundary to curb offloading cost; as the link recovers, the boundary lifts to exploit cloud quality gains. The utility series shows smooth piecewise transitions without overshoot or oscillations, indicating stable adaptation under non-stationary links.

C. Quality-Cost Frontier and Network Sensitivity

Fig. 7 reports the attainable quality-cost frontiers by sweeping the fallback threshold τ under three fixed network conditions (GOOD, MID, BAD). The curves are smooth, monotonic in cost, and show diminishing marginal quality gains as cost increases, empirically supporting the decreasing-benefit Assumption 2 used in our analysis. Consistent with Eq. (27), at the same fallback threshold, the frontier slope scales as $1/\kappa(S)$, so degraded links (larger κ) flatten the curve and shift it rightward/downward relative to better network states. Across regimes, the frontier shifts rightward (and slightly downward)

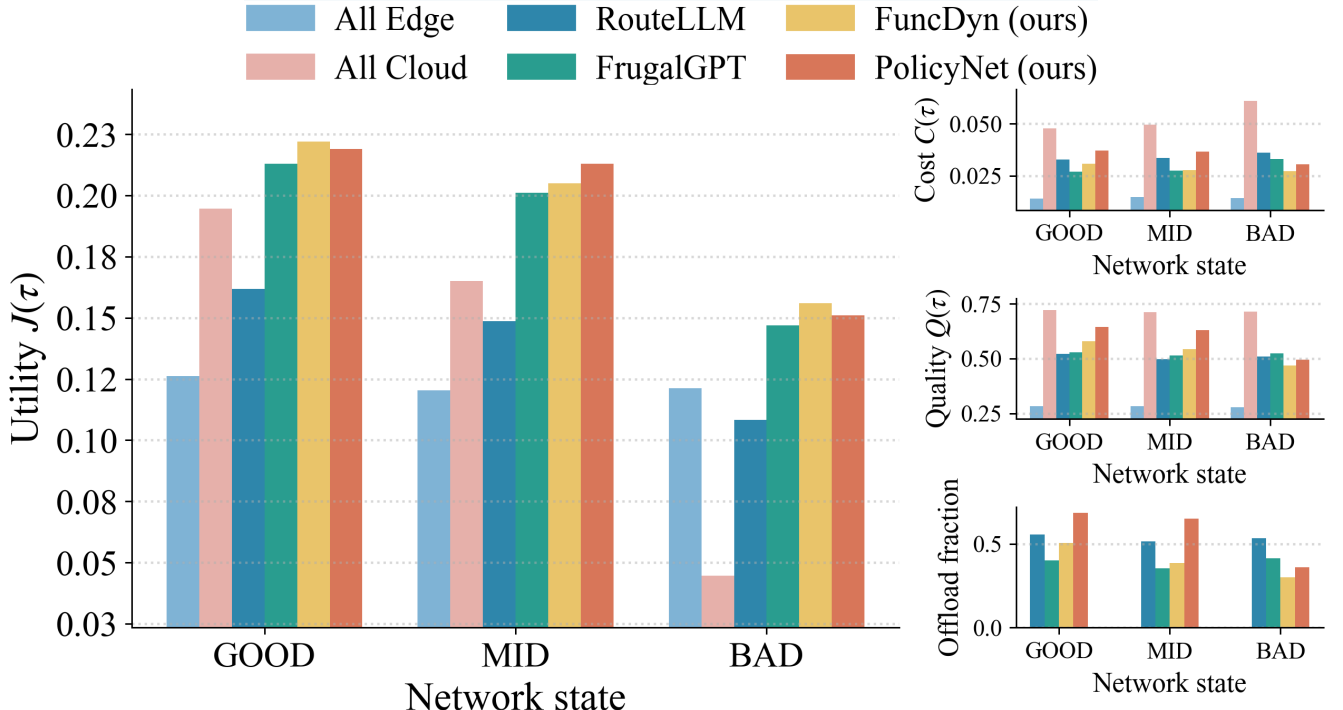


Fig. 5: Comparison among All Edge, All Cloud, RouteLLM [14], FrugalGPT [11], and the dynamic controllers (FuncDyn, PolicyNet) under GOOD/MID/BAD links.

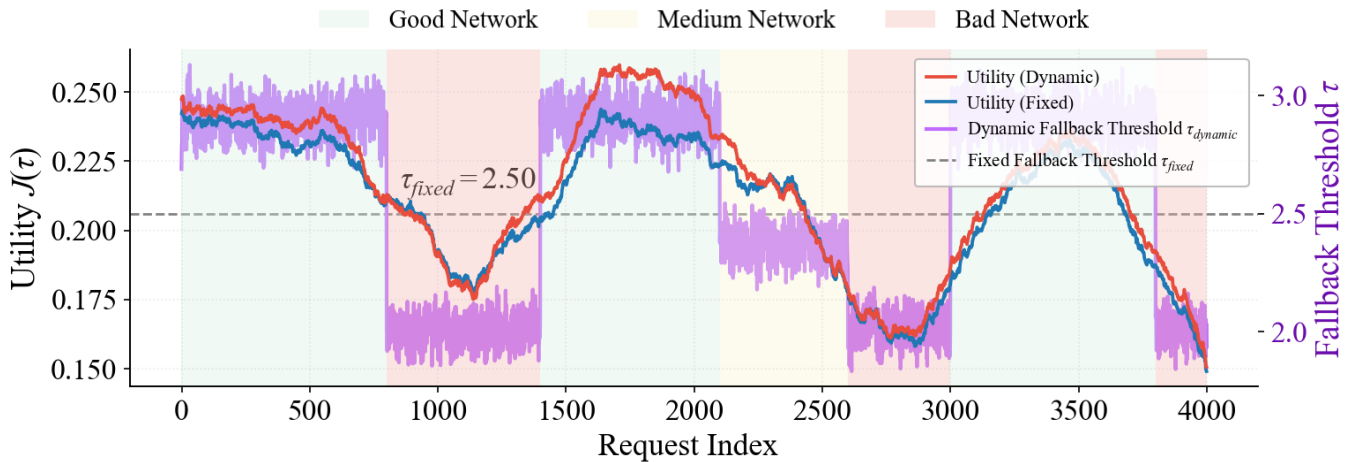


Fig. 6: Dynamic vs. fixed fallback threshold under time-varying links.

from GOOD to BAD, indicating that worse links require more cost to reach the same quality and deliver lower quality at the same cost—consistent with our theory that degraded networks raise the effective offloading cost and push decisions toward edge execution.

Fig. 8 shows the sensitivity of the score-threshold policy to network conditions. We sweep the fallback threshold τ under three network regimes while fixing the trade-off weight at $\lambda = 10$, and plot the resulting quality, cost, and utility curves. As RTT increases and bandwidth decreases from GOOD to MID to BAD, both curves shift, and the utility-maximizing fallback threshold moves leftward. The empirical optima $\tau_{GOOD}^* \approx 4.54$, $\tau_{MID}^* \approx 4.28$, and $\tau_{BAD}^* \approx 3.59$

follow the monotone comparative-statics pattern predicted by our analysis: deteriorating links impose higher communication costs, which discourage cloud offloading and favor more permissive local acceptance at the edge. These results confirm that the proposed score-threshold policy adapts smoothly and predictably as link quality worsens.

For completeness, Fig. 9 further decomposes the fallback threshold scan by plotting $Q(\tau)$ and $C(\tau)$ together with overlaid utility curves $J(\tau)$ for different values of λ . Across all settings, the $J(\tau)$ profiles remain unimodal, and the maximizing fallback threshold shifts leftward as λ increases, reflecting heightened sensitivity to cost.

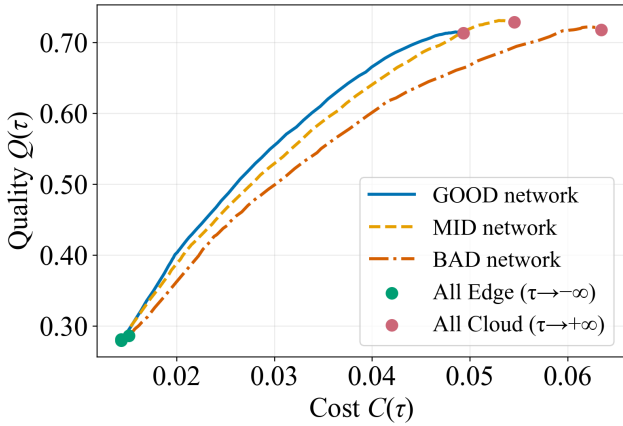


Fig. 7: Quality-Cost frontiers across fixed network regimes.

D. Effectiveness of PPO-based Learning

We assess the effectiveness of on-device policy optimization with the SFT anchor to preserve schema-correct tool-calling. Fig. 10 contrasts training with and without the SFT anchor. It can be observed that the involvement of SFT leads to monotonically increased reward with lower variance and a steadily declining offload rate, indicating reliable improvement without structural drift. These results corroborate that interleaved SFT updates stabilize RL by constraining updates around a schema-preserving reference. Fig. 11 shows the quality-cost frontier before and after PPO training. After training, the frontier strictly dominates the pre-training curve across a range of λ values, suggesting that the utility gains are robust and not tied to a single trade-off weight. From a multi-agent perspective, the router, the edge LLM policy, and the cloud model operate in a network feedback loop. The improvements in Fig. 10 and the shift of the quality-cost frontier in Fig. 11 are consistent with coordinated updates driven by online feedback rather than offline tuning alone.

To quantify the router’s scoring quality, we examine risk-coverage curves [42] before and after RM training. Notably, for a fallback threshold τ , the *coverage* is the fraction of requests accepted at the edge, while *selective risk* is the fraction of these accepted cases for which the cloud would have produced a better result (i.e., should-have-offloaded errors). As shown in Fig. 12, the post-training curve lies uniformly below the pre-training curve, especially in the medium-to-high coverage range, demonstrating sharper discrimination near the decision boundary.

VI. CONCLUSION AND FUTURE WORK

We have introduced a network-aware LLM routing framework that unifies schema-constrained tool planning at the edge with a router-as-reward loop for continual improvement. We have cast offloading as state-dependent thresholding of a unified RM score, aligning routing, cost, and quality through a single, interpretable fallback threshold adapted to the network state. We have implemented two deployable variants—FuncDyn and a lightweight PolicyNet—both adapting online to time-varying links with minimal overhead. We have

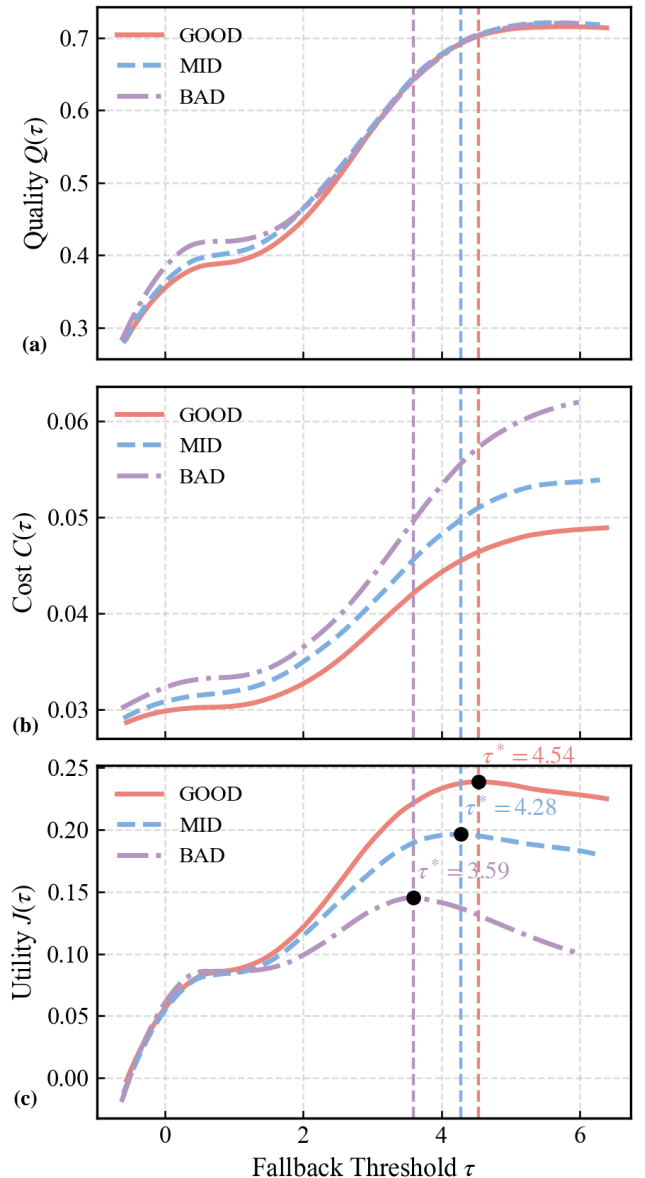


Fig. 8: Network sensitivity of the score-threshold policy. (a) Composite quality $Q(\tau)$, (b) total cost $C(\tau)$, and (c) utility $J(\tau) = Q - \lambda C$ under the three network states.

established the existence and uniqueness of the optimal fallback threshold and derived monotone comparative statics with respect to bandwidth and RTT. Furthermore, we have validated the effectiveness and superiority across extensive simulations. Subsequent research will investigate multi-edge/multi-cloud orchestration with cooperative routers and a shared reward model, robustness of reward signals under distribution shift, and hardware-in-the-loop evaluations on real network traces.

APPENDIX A INITIALIZATION OF EDGE POLICY, RM, AND FALBACK THRESHOLD

We initialize the edge LLM policy π_θ , the reward/router model g_ψ that outputs the score $s_{i,k}$, and a fixed fallback threshold τ_0 for runtime use.

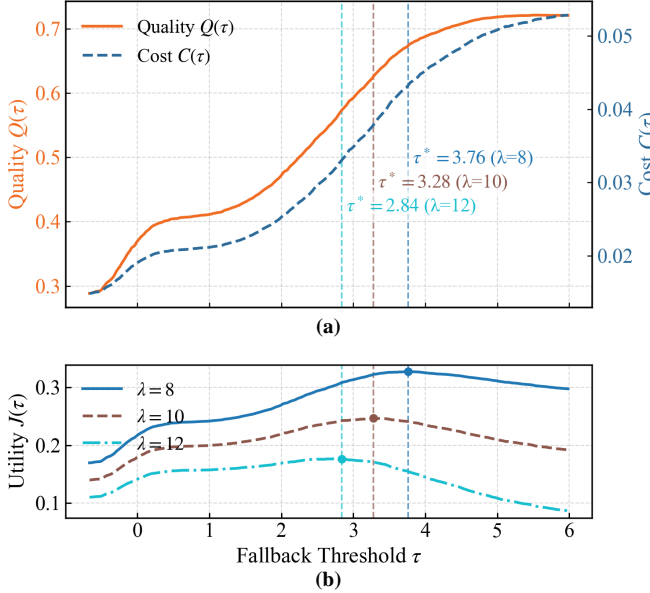


Fig. 9: Fallback threshold scan: $Q(\tau)$, $C(\tau)$, and $J(\tau)$ for $\lambda \in \{8, 10, 12\}$; vertical lines indicate τ^* for each λ .

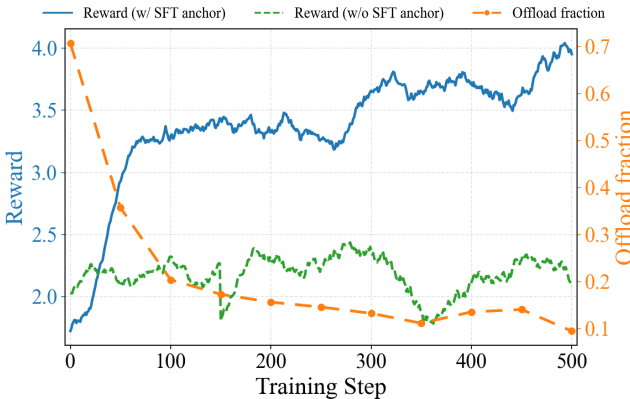


Fig. 10: PPO with vs. without SFT anchoring. Router-reward trends and offload rate over training steps.

Particularly, we fit π_θ on traces $(x_i, H_{i,k}, u_{i,k})$ with supervised cross-entropy:

$$\mathcal{L}_{\text{SFT}}(\theta) = \mathbb{E}[-\log \pi_\theta(u_{i,k} | x_i, H_{i,k})]. \quad (37)$$

Here x_i is the task input, $H_{i,k}$ is the historical step, and $u_{i,k} = (\text{tool}, \text{args}, \text{thought})$ is the teacher action that satisfies the schema.

The reward model outputs a scalar score $s_{i,k} = g_\psi(x_i, H_{i,k}, u_{i,k}) \in \mathbb{R}$ for routing and as the learning reward. We initialize g_ψ with a pairwise ranking loss:

$$\mathcal{L}_{\text{RM}}(\psi) = \mathbb{E} \left[\log(1 + \exp(-(s_{i,k}^+ - s_{i,k}^-))) \right]. \quad (38)$$

Here $s_{i,k}^+$ and $s_{i,k}^-$ are the RM scores of a preferred and a non-preferred answer under the same context $(x_i, H_{i,k})$. The preferred answers come from the cloud LLM outputs, while the non-preferred ones are generated by the edge LLM after SFT initialization. This construction lets the RM learn the

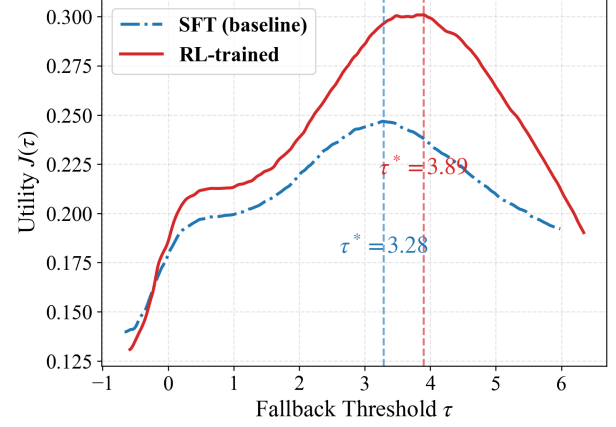


Fig. 11: Utility comparison before and after RL.

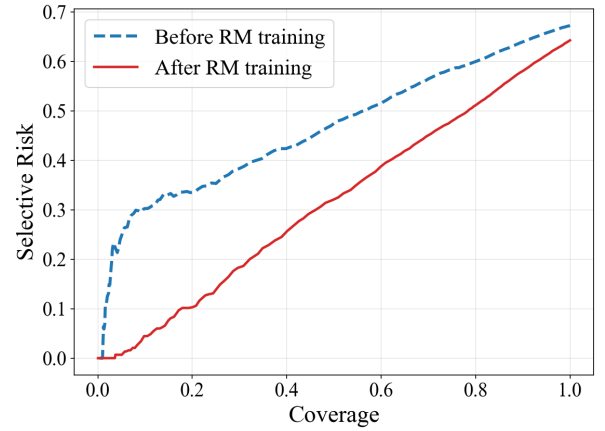


Fig. 12: RM Risk-Coverage curves before vs. after training. Post-training curves reduce risk at fixed coverage, indicating more accurate router scoring near the decision boundary.

quality gap between edge and cloud responses under identical conditions.

We select an initial fallback threshold τ_0 on an offline dataset $\mathcal{D}_{\text{init}}$. Each record in $\mathcal{D}_{\text{init}}$ provides the score $s_{i,k}$ and the empirical utilities we would obtain by choosing edge or cloud at that step:

$$J_{i,k}^{\text{edge}} \triangleq Q_{i,k}^{\text{edge}} - \lambda C_{i,k}^{\text{edge}}, \quad J_{i,k}^{\text{cloud}} \triangleq Q_{i,k}^{\text{cloud}} - \lambda C_{i,k}^{\text{cloud}}. \quad (39)$$

Here $Q_{i,k} \in [0, 1]$ and $C_{i,k} \geq 0$ denote the measured quality and the step-level cost (e.g., latency or monetary cost), respectively. $\lambda > 0$ is the trade-off weight. We then choose τ_0 by empirical utility maximization under the hard fallback threshold rule:

$$\begin{aligned} \tau_0 & \in \arg \max_{\tau \in \mathbb{R}} \sum_{(i,k) \in \mathcal{D}_{\text{init}}} \left[J_{i,k}^{\text{edge}} \mathbb{I}[s_{i,k} \geq \tau] + J_{i,k}^{\text{cloud}} \mathbb{I}[s_{i,k} < \tau] \right], \end{aligned} \quad (40)$$

which picks the fixed fallback threshold that yields the highest average utility on $\mathcal{D}_{\text{init}}$.

Our training datasets are batch-generated with GPT-4o

Listing 1: SFT sample with structured tool call.

```

1  {
2      "query": "Optimize a federated
3          recommendation system for news articles
4          across mobile devices.",
5      "completed_steps": [
6          "initialize_nodes"
7      ],
8      "thought": "After initializing nodes, we
9          need to simulate the network topology.
10         Since this involves mobile devices, we
11         should account for variable bandwidth
12         and latency. This will help model
13         realistic communication conditions
14         during federated training.",
15      "output": {
16          "name": "simulate_topology",
17          "args": {
18              "node_count": 5,
19              "bandwidth_limits": "10-100 Mbps",
20              "latencies": "50-200ms"
21          }
22      },
23      "available_tools": [
24          "initialize_nodes(node_count, model_class,
25              dataset_name)",
26          "simulate_topology(node_count,
27              bandwidth_limits, latencies)",
28          "train_local_models(nodes, dataset, epochs
29              , batch_size, learning_rate)",
30          "train_local_models_fedprox(nodes, dataset
31              , global_model, mu, epochs, batch_size
32              , learning_rate)",
33          "train_local_models_secure_agg(nodes,
34              dataset, epochs, batch_size,
35              learning_rate)",
36          "aggregate_global_model(local_models,
37              weights, nodes, dataset, topology)",
38          "aggregate_global_model_krum(local_models,
39              num_selected, nodes, dataset,
40              topology)",
41          "aggregate_global_model_median(
42              local_models, nodes, dataset, topology
43              )",
44          "aggregate_global_model_secure_agg(
45              local_models, nodes, dataset, topology
46              )",
47          "finish()"
48      ]
49  }

```

Listing 2: Preference pair: chosen vs. rejected sample.

```

1  {
2      "input": {
3          "query": "Stanford medical researchers
4              require federated training of a 3D U-
5              Net for brain tumor segmentation
6              across 7 hospitals, with differential
7              privacy epsilon=0.5 guarantees.",
8          "completed_steps": []
9      },
10     "chosen": {
11         "action": {
12             "name": "initialize_nodes",
13             "args": {
14                 "node_count": 8,
15                 "model_class": "3D U-Net",
16                 "dataset_name": "brain_tumor_segmentation"
17             }
18         },
19         "thought": "First initialize the federated
20             learning nodes with the 3D U-Net
21             model and brain tumor segmentation
22             dataset. Next steps will involve
23             setting up the network topology and
24             beginning the federated training
25             process with differential privacy
26             guarantees. Need to ensure the model
27             class and dataset name are correctly
28             specified for the medical imaging task
29             . Initializing 8 nodes (7 hospitals +
30             central server) with 3D U-Net models
31             for brain tumor segmentation."
32     },
33     "rejected": {
34         "action": {
35             "name": "initialize_nodes",
36             "args": {
37                 "node_count": 7,
38                 "model_class": "MedicalImagingModel",
39                 "dataset_name": "TumorScans"
40             }
41         },
42         "thought": "Starting fresh with this
43             sensitive medical task. We'll
44             initialize 7 nodes (one per hospital)
45             with a specialized medical imaging
46             model. Using a small batch size (16)
47             to handle potentially limited patient
48             data at each site."
49     }
50  }

```

[43], yielding 8,000 SFT instances for schema-faithful initialization and 2,000 preference pairs for reward modeling. In addition, we generate 8,000 tasks for inference experiments and simulated continual improvement. To ensure diversity, each batch draws a prompt *uniformly at random* from a maintained pool containing multiple prompt templates. Every template rigidly specifies the output schema (tool name, arguments, and brief thought trace) to match our tool-calling interface. After generation, we run a two-stage filtering pass: (i) schema validation (JSON/tool-slot conformance and argument type checks), and (ii) quality screening (automatic scoring to eliminate near-duplicates and low-utility samples). The resulting corpora include: (a) *SFT data*, used to initialize

schema-faithful tool use for the edge agent; and (b) *preference pairs*, where a *chosen* action (typically the cloud-produced response) is contrasted with a *rejected* action (typically an edge-produced alternative) under the same context, supporting reward modeling and preference optimization.

APPENDIX B CACHING SETUP AND ON-POLICY LOGGING

With DeepSeek-V3.2-Exp as the fallback cloud LLM, the cached records serve multiple purposes in the learning pipeline:

- Cloud-offloaded traces provide training data for improving the edge LLM through RL.
- Near-threshold cloud cases, together with the small set of above-threshold samples intentionally uploaded, constitute a focused dataset for refining the reward model around the decision boundary.
- Execution outputs contribute to prompt construction: edge-side prompts append only the executed tool name to `completed_steps`, whereas cloud-side prompts additionally include a concise natural-language summary.

Therefore, we denote the cached tuple by

$$\mathcal{T}_{i,k} \triangleq (x_i, H_{i,k}, u_{i,k}, u_{i,k}^*, s_{i,k}).$$

Only steps offloaded to the cloud ($d_{i,k} = \text{CLOUD}$) append $\mathcal{T}_{i,k}$ to the local cache \mathcal{B}_{RM} and \mathcal{B}_{RL} for later updates; on-device steps retain only $H_{i,k}$.

To enrich the reward model’s learning signal, we randomly sample a small fraction of steps whose scores are slightly above the fallback threshold, i.e., $s_{i,k} \gtrsim \tau(S_{i,k})$, and also upload them to the cloud. These near-threshold samples capture marginal decision cases that are most informative for distinguishing good and bad routing choices. After executing the selected tool, we record a structured output

$$o_{i,k} = (t_{i,k}, \sigma_{i,k}), \quad (41)$$

where $t_{i,k}$ is the tool identifier and $\sigma_{i,k}$ is a length-bounded summary of the tool output (sufficient for the next-step LLM to interpret the result while keeping context compact).

The incorporation of $o_{i,k}$ into the local state depends on which model the next prompt is constructed for: edge-side prompts use only the tool identifier, whereas cloud-side prompts include both the identifier and its summary. Formally,

$$H_{i,k+1} = \begin{cases} H_{i,k} \oplus t_{i,k}, & \text{to edge LLM,} \\ H_{i,k} \oplus (t_{i,k}, \sigma_{i,k}), & \text{to cloud LLM.} \end{cases} \quad (42)$$

Here \oplus denotes concatenation into the reasoning trace.

REFERENCES

- [1] Y. Chen, R. Li, *et al.*, “NetGPT: An AI-native network architecture for provisioning beyond personalized generative services,” *IEEE Network*, vol. 38, no. 6, pp. 404–413, 2024.
- [2] OpenAI, “Function calling and other api updates,” Online blog post, Jun 2023. [Online]. Available: <https://openai.com/index/function-calling-and-other-api-updates/>
- [3] S. Yao, J. Zhao, *et al.*, “ReAct: Synergizing reasoning and acting in language models,” in *Proceedings of the 11th International Conference on Learning Representations (ICLR 2023)*, Kigali, Rwanda, May 2023.
- [4] W. Shi, J. Cao, *et al.*, “Edge computing: Vision and challenges,” *IEEE Internet of Things Journal*, vol. 3, no. 5, p. 637–646, 2016.
- [5] E. Li, Z. Zhou, *et al.*, “Edge intelligence: On-demand deep learning model co-inference with device-edge synergy,” in *Proceedings of the 2018 Workshop on Mobile Edge Communications (MECOMM@SIGCOMM)*, August 2018, pp. 31–36.
- [6] P. Mach and Z. Becvar, “Mobile edge computing: A survey on architecture and computation offloading,” *IEEE Communications Surveys & Tutorials*, vol. 19, no. 3, pp. 1628–1656, 2017.
- [7] L. Ouyang, J. Wu, *et al.*, “Training language models to follow instructions with human feedback,” in *Proceedings of the 36th International Conference on Neural Information Processing Systems (NeurIPS 2022)*, Red Hook, NY, USA, December 2022, pp. 2011–2021.
- [8] O. Besbes, Y. Gur, *et al.*, “Stochastic multi-armed-bandit problem with non-stationary rewards,” in *Proceedings of the 28th Conference on Neural Information Processing Systems (NIPS 2014)*, Cambridge, MA, USA, 2014, p. 199–207.
- [9] T. Schick, J. Dwivedi-Yu, *et al.*, “Toolformer: Language models can teach themselves to use tools,” *arXiv preprint arXiv:2302.04761*, 2023.
- [10] B. Agarwal, I. Joshi, *et al.*, “Think inside the json: Reinforcement strategy for strict LLM schema adherence,” *arXiv preprint arXiv:2502.14905*, 2025.
- [11] L. Chen and M. Zaharia, “FrugalGPT: How to use large language models while reducing cost and improving performance,” in *Transactions on Machine Learning Research (TMLR) Workshop Track*, Online, December 2024.
- [12] K. Lu, H. Yuan, *et al.*, “Routing to the expert: Efficient reward-guided ensemble of large language models,” in *Proceedings of the Conference of the North American Chapter of the Association for Computational Linguistics: Human Language Technologies (NAACL-HLT 2024)*, Mexico City, Mexico, June 2024, pp. 1964–1974.
- [13] H. Zheng, H. Xu, *et al.*, “Disrouter: Distributed self-routing for LLM selections,” *arXiv preprint arXiv:2510.19208*, 2025.
- [14] I. Ong, A. Almahairi, *et al.*, “RouteLLM: Learning to route llms from preference data,” in *Proceedings of the 13th International Conference on Learning Representations (ICLR 2025)*, Singapore EXPO, Singapore, April 2025.
- [15] D. Ding, A. Mallick, *et al.*, “Hybrid-LLM: Cost-efficient and quality-aware query routing,” in *Proceedings of the 12th International Conference on Learning Representations (ICLR 2024)*, Vienna, Austria, May 2024.
- [16] S. Chen, W. Jiang, *et al.*, “Routerde: Query-based router by dual contrastive learning for assembling large language models,” in *Proceedings of the 37th Annual Conference on Neural Information Processing Systems (NeurIPS 2024)*, vol. 37, Vancouver, Canada, 2024, pp. 66305–66328.
- [17] T. Feng, Y. Shen, *et al.*, “Graphrouter: A graph-based router for LLM selections,” in *Proceedings of the 13th International Conference on Learning Representations (ICLR 2025)*, Singapore EXPO, Singapore, April 2025.
- [18] Y. Yue, G. Zhang, *et al.*, “Masrouter: Learning to route llms for multi-agent systems,” in *Proceedings of the 63rd Annual Meeting of the Association for Computational Linguistics (Volume 1: Long Papers)*, Vienna, Austria, July 2025, pp. 15549–15572.
- [19] B. Qi, P. Li, *et al.*, “Online direct preference optimization with fast–slow memory,” *arXiv preprint arXiv:2406.05534*, 2024.
- [20] H. Dong, W. Xiong, *et al.*, “RLHF workflow: From reward modeling to online RLHF,” *arXiv preprint arXiv:2405.07863*, 2024.
- [21] X. Wang, Y. Liu, *et al.*, “MixLLM: Dynamic routing in mixed large language models,” in *Proceedings of the 2025 Conference of the North American Chapter of the Association for Computational Linguistics: Human Language Technologies (NAACL-HLT 2025)*, Albuquerque, New Mexico, 2025, pp. 10912–10922.
- [22] Q. H. Nguyen, T. Dao, *et al.*, “MetaLLM: A high-performant and cost-efficient dynamic framework for wrapping LLMs,” *arXiv preprint arXiv:2407.10834*, 2024.
- [23] J. Schulman, F. Wolski, *et al.*, “Proximal policy optimization algorithms,” *arXiv preprint arXiv:1707.06347*, 2017.
- [24] Q. J. Hu, J. Bicker, *et al.*, “Routerbench: A benchmark for multi-LLM routing system,” *arXiv preprint arXiv:2403.12031*, 2024.
- [25] J. Dekoninck, M. Baader, *et al.*, “A unified approach to routing and cascading for LLMs,” in *Proceedings of the First Workshop on Scalable Optimization for Efficient and Adaptive Foundation Models (SCOPE), co-located with ICLR 2025*, Singapore Expo, Singapore, April 2025.
- [26] M. Yue, J. Zhao, *et al.*, “Large language model cascades with mixture of thought representations for cost-efficient reasoning,” in *Proceedings of the 12th International Conference on Learning Representations (ICLR 2024)*, Vienna, Austria, May 2024.
- [27] Y. Shen, Y. Liu, *et al.*, “Sater: A self-aware and token-efficient approach to routing and cascading,” in *Proceedings of the 2025 Conference on Empirical Methods in Natural Language Processing (EMNLP 2025)*, Suzhou, China, November 2025, pp. 10526–10540.
- [28] D. Ding, A. Mallick, *et al.*, “Best-route: Adaptive LLM routing with test-time optimal compute,” in *Proceedings of the 42nd International Conference on Machine Learning (ICML 2025) Poster*, 2025.
- [29] Y. Li, “Rethinking predictive modeling for LLM routing: When simple knn beats complex learned routers,” *arXiv preprint arXiv:2505.12601*, 2025.
- [30] D. Calandriello, Z. D. Guo, *et al.*, “Human alignment of large language models through online preference optimisation,” in *Proceedings of the*

41st International Conference on Machine Learning (ICML 2024), Vienna, Austria, 2024.

- [31] W. Yuan, R. Y. Pang, *et al.*, “Self-rewarding language models,” in *Proceedings of the 41st International Conference on Machine Learning (ICML 2024)*, Vienna, Austria, July 2024, pp. 57905–57923.
- [32] Z. Wang, W. He, *et al.*, “Cream: Consistency regularized self-rewarding language models,” in *Proceedings of the 13th International Conference on Learning Representations (ICLR 2025)*, Singapore EXPO, Singapore, April 2025.
- [33] Y. Wu, Z. Sun, *et al.*, “Self-play preference optimization for language model alignment,” in *Proceedings of the 13th International Conference on Learning Representations (ICLR 2025)*, Singapore EXPO, Singapore, April 2025.
- [34] S. S. Ramesh, Y. Hu, *et al.*, “Group robust preference optimization in reward-free rlhf,” in *Proceedings of the 38th Conference on Neural Information Processing Systems (NeurIPS 2024)*, Vancouver, BC, Canada, December 2024, pp. 37100–37137.
- [35] Z. Shao, P. Wang, *et al.*, “Deepseekmath: Pushing the limits of mathematical reasoning in open language models,” *arXiv preprint arXiv:2402.03300*, 2024.
- [36] C. Ye, W. Xiong, *et al.*, “Online iterative reinforcement learning from human feedback with general preference model,” in *Proceedings of the 38th Conference on Neural Information Processing Systems (NeurIPS 2024)*, Vancouver, BC, Canada, December 2024.
- [37] *Network performance objectives for IP-based services*, International Telecommunication Union, Telecommunication Standardization Sector (ITU-T) Std. Y.1541, Dec. 2011, recommendation ITU-T Y.1541 (12/2011). [Online]. Available: https://www.itu.int/rec/dologin_pub.asp?id=T-REC-Y.1541-201112-I!!PDF-E&lang=e&type=items
- [38] B. Constantine, G. Forget, *et al.*, “Framework for TCP Throughput Testing,” RFC 6349, August 2011. [Online]. Available: <https://www.rfc-editor.org/info/rfc6349>
- [39] M. Geist, B. Scherrer, *et al.*, “A theory of regularized Markov decision processes,” in *Proceedings of the 36th International Conference on Machine Learning (ICML 2019)*, Long Beach, USA, June 2019, pp. 2160–2169.
- [40] A. Banerjee, S. Merugu, *et al.*, “Clustering with bregman divergences,” *Journal of Machine Learning Research*, vol. 6, no. 58, pp. 1705–1749, 2005.
- [41] S. Ghandour-Haidar, L. Ros, *et al.*, “On the use of first-order autoregressive modeling for rayleigh flat fading channel estimation with kalman filter,” *Signal Processing*, vol. 92, no. 2, pp. 601–606, 2012.
- [42] R. El-Yaniv and Y. Wiener, “On the foundations of noise-free selective classification,” *Journal of Machine Learning Research*, vol. 11, pp. 1605–1641, 2010.
- [43] OpenAI, “GPT-4o technical report,” <https://openai.com/research/gpt-4o>, 2024, accessed: 2025-11-20.